Stochastic resonance in models of neuronal ensembles

Dante R. Chialvo,[1,3] André Longtin,[2] and Johannes Müller-Gerking[1]
[1]*Division of Neural Systems, Memory and Aging, University of Arizona, Tucson, Arizona 85724*
[2]*Département de Physique, Université d'Ottawa, 150 Louis Pasteur, Ottawa, Ontario, Canada K1N 6N5*
[3]*Santa Fe Institute, 1399 Hyde Park Road, Santa Fe, New Mexico 87501*
(Received 30 July 1996; revised manuscript received 18 October 1996)

Two recently suggested mechanisms for the neuronal encoding of sensory information involving the effect of stochastic resonance with aperiodic time-varying inputs are considered. It is shown, using theoretical arguments and numerical simulations, that the nonmonotonic behavior with increasing noise of the correlation measures used for the so-called aperiodic stochastic resonance (ASR) scenario does not rely on the cooperative effect typical of stochastic resonance in bistable and excitable systems. Rather, ASR with slowly varying signals is more properly interpreted as linearization by noise. Consequently, the broadening of the ''resonance curve'' in the multineuron *stochastic resonance without tuning* scenario can also be explained by this linearization. Computation of the input-output correlation as a function of both signal frequency and noise for the model system further reveals conditions where noise-induced firing with aperiodic inputs will benefit from stochastic resonance rather than linearization by noise. Thus, our study clarifies the tuning requirements for the optimal transduction of subthreshold aperiodic signals. It also shows that a single deterministic neuron can perform as well as a network when biased into a suprathreshold regime. Finally, we show that the inclusion of a refractory period in the spike-detection scheme produces a better correlation between instantaneous firing rate and input signal. [S1063-651X(97)01102-1]

PACS number(s): 87.10.+e

I. INTRODUCTION

''Stochastic resonance (SR) is a term which describes the coincidence of *two* time scales in a periodically modulated multistable, stochastic system. One time scale is established by the period of the external stimulus and the other by the well-to-well switching rate induced by the stochastic process or noise'' [1]. By this effect, the synchronization of a nonlinear system to a weak periodic signal can be enhanced by the presence of random fluctuations. A weak periodic signal is one which cannot by itself produce switchings between wells. The optimum enhancement is obtained at a level of noise which produces a maximum cooperative (i.e.,''resonance'') effect between the noise-induced transitions between wells and the frequency of the deterministic periodic signal [2]. Thus, the noise level producing the optimum synchronization always depends to some extent on the frequency of the periodic signal.

It is well known that biological sensory receptors transform analog quantities such us pressure, temperature, electric field, etc., into trains of action potentials or ''spikes.'' The information about the physical stimuli is encoded in the time intervals between spikes. All the features of systems exhibiting SR were found to be present in sensory neurons [3], which are intrinsically noisy, nonlinear threshold systems. In such systems the essence of the signal-enhancing effect of SR can be simply grasped. In the absence of stimuli, there are random threshold crossings, each of which results in a spike. The mean time between crossings decreases as the noise intensity increases. A weak subthreshold deterministic modulation will then be best expressed in the output spike train if its dominant frequency is close to the noise-induced mean spiking rate in the absence of signal.

Further theoretical and experimental work on single and multineuron systems [4] has provided additional examples of circumstances in which neuronal synchronization is enhanced by some level of random fluctuations. In the context of harmonically forced neurons, the signal-to-noise ratio (SNR) has typically been used to quantify the noise-induced synchronization of the neuron firings to the subthreshold signal. The precise resonant behavior of this SNR as a function of noise intensity depends on signal characteristics such as bias, frequency, amplitude, as well as on parameters governing the autonomous neural dynamics and the noise. This implies that an optimal response to a signal of varying characteristics could be maintained if the sensory neuron somehow ''tunes'' or adapts itself accordingly [5].

In a recent paper, Collins *et al.* [6] showed that a single noisy neuron can also optimally transduce a subthreshold slowly varying aperiodic signal, such as low-pass filtered noise (see below). Their study proposed SR measures appropriate for characterizing this so-called ''aperiodic stochastic resonance'' effect (ASR). The proposed power norm C_0 and normalized power norm C_1 measure the quality of the transduction by the correlation between input signal and output instantaneous firing rate. In this setting, a ''resonance curve'' of correlation versus noise intensity was obtained which resembled those for SR: with increasing noise, the correlation rose sharply to a peak, and dropped thereafter (Fig. 4; cf. [6], Fig. 1). These authors also recognized that for ASR, while restrictions on frequency are relaxed due to the use of slowly varying signals, it would still be necessary to modulate or actively ''tune'' the noise intensity (or other parameters) in order to optimally transduce a signal whose characteristics (such as mean level, variance, etc.) change with time.

Another recent report [7] analyzed the extension of the single neuron ASR property to a population of noisy neurons acting in parallel on the same aperiodic input signal. The

aforementioned C_1 was then computed using the signal and the average instantaneous firing rate of these neurons. It was shown that this measure asymptotically approaches one with increasing number of neurons, whenever the noise level is above a certain minimum (Fig. 6; cf. [7], Fig. 2). This *stochastic resonance without tuning* effect suggested that populations of neurons acting in parallel could, apparently, use SR and still overcome the tuning problem. In a restricted sense, the connection to tuning relates to the ''time-scale matching'' notion of SR, in which one noise intensity optimally transduces a given frequency; hence, high correlation over a wide range of noise intensities could transduce a wide-band input signal. In a larger sense, tuning refers to adjusting all system and noise parameters to optimally detect a signal; their results would then imply that the noise-averaging property of the summing network makes this tuning less critical.

These two reports suggest that neurons could use SR to optimize their output coherence with weak input signals, regardless of frequency in the case of a single neuron, and of frequency and noise intensity in the case of summing networks. Being the essence of SR, the coincidence of *two* time scales [1,2], achieving enhancement of the signal by the noise for a wide range of frequencies (i.e., ''aperiodic stochastic resonance'') and/or noise intensities (i.e., ''stochastic resonance without tuning'') implies either a paradox or a misinterpretation.

The aim of this paper is to show, through a simple analysis, that the nonmonotonic correlation-versus-noise relationship associated with aperiodic stochastic resonance and stochastic resonance without tuning does not rely on the cooperative effect typical of SR. Rather, it is a consequence of linearization-by-noise of the transfer function that relates ''mean firing rate'' to ''activation level.'' The match between our theory and the simulations shows that the role of the noise in ASR with slowly varying inputs is to produce a positive linear gain for the nonlinear threshold element in a region of otherwise quiescent dynamics. Our analysis is based on the same assumption as that for ASR [6], namely, that the time variations of the input signal occur on a time scale which is slower than all characteristic times of the neuron(s).

The excitable neuron model, which closely follows that in [6], is introduced in Sec. II. Some technical points regarding spike detection, relevant in later sections, are also presented in this section. Section III is dedicated to replicating the numerical results in [6,7] which are relevant to our study. The fundamental diagram of mean firing rate-versus-noise intensity is introduced in Sec. IV. In Sec. V, expressions for the expected values of the covariance and correlation coefficient in the quasistatic case (i.e., for slowly varying inputs) are derived and compared with the numerical simulations of the full dynamics. Section VI places the results of the preceding sections in the light of the dependence of the SNR on noise and frequency for the case of pure harmonic signals. The paper concludes in Sec. VII.

II. MODEL AND NUMERICAL CONSIDERATIONS

We consider the FitzHugh-Nagumo (FHN) neuronal model driven by a subthreshold signal and noise [8]. Subthreshold means that the driving signal alone is not of sufficient amplitude to produce action potentials. The system equations are

$$\epsilon\dot{v} = v(v-a)(1-v) - w + A + S(t) + \zeta(t),$$

$$\dot{w} = v - w - b, \tag{2.1}$$

where $v(t)$ is a fast (voltage) variable and $w(t)$ is a slow (recovery) variable. The parameters are chosen as in [6,7], namely, A is a constant (tonic) activation set to 0.04 (unless otherwise stated), $\epsilon = 0.005, a = 0.5$, and $b = 0.15$. $S(t)$ is the aperiodic signal. $\zeta(t)$ is the noise given by an Ornstein-Uhlenbeck (OU) stochastic process of the form

$$\dot{\zeta}(t) = -\lambda\zeta(t) + \lambda\xi(t), \tag{2.2}$$

where $\xi(t)$ is Gaussian white noise of zero mean and correlation $\langle \xi(t)\xi(s)\rangle = 2D\delta(t-s)$. The autocorrelation of the OU process is given by

$$\langle \zeta(t)\zeta(s)\rangle = (D/\tau_c)\exp(-|t-s|/\tau_c) \tag{2.3}$$

and its variance is D/τ_c. The choice of a OU process allows control over both noise intensity (referred to throughout as D rather than D/τ_c) and correlation time $\tau_c = \lambda^{-1}$.

We integrated (with a fixed step size of 0.001 sec) the deterministic system Eq. (2.1) coupled to the OU process Eq. (2.2) using a fourth-order Runge-Kutta method for the deterministic equations, while the algorithm in [9] provides an accuracy of the noise integration of order 3/2. This integration scheme suffices for our purpose of reproducing Collins *et al.* [6,7] results. However, if the interest is in a more precise solution, the integration methods in [10] are more appropriate.

A good approximation to Gaussian white noise is obtained by choosing τ_c equal to the integration step size. The positive-going excursions of $v(t)$ reaching a minimum amplitude (here set to 0.5 as in [8]) are considered as action potentials with the caveats discussed in the next subsection. The times of occurrence of the action potentials form a point process which is modeled as a train of equal-amplitude δ-function spikes. This spike train is then convolved with a 10 sec unit-area symmetric Hanning window in order to obtain an instantaneous firing rate that varies in time. The convolved spike train constitutes the output signal $R(t)$.

Spike detection schemes

Adopting the upward threshold crossing of $v(t)$ as the only criterion for spike detection presents a problem for the mid-to-high noise intensities considered in our study. For these intensities, $v(t)$ can fluctuate rapidly several times around the threshold.

Consider, for instance, the case depicted in panel (a) of Fig. 1, where the time course of $v(t)$ is plotted. With the aforementioned parameters, no spikes are produced in the absence of noise. With noise, we find that an action potential is induced starting at around time 15.82 sec, and evolves for about 300 msec. There are two additional threshold crossings preceding this action potential (indicated by the vertical bars) with interspike intervals of 3 and 2 msec. It is known that, in

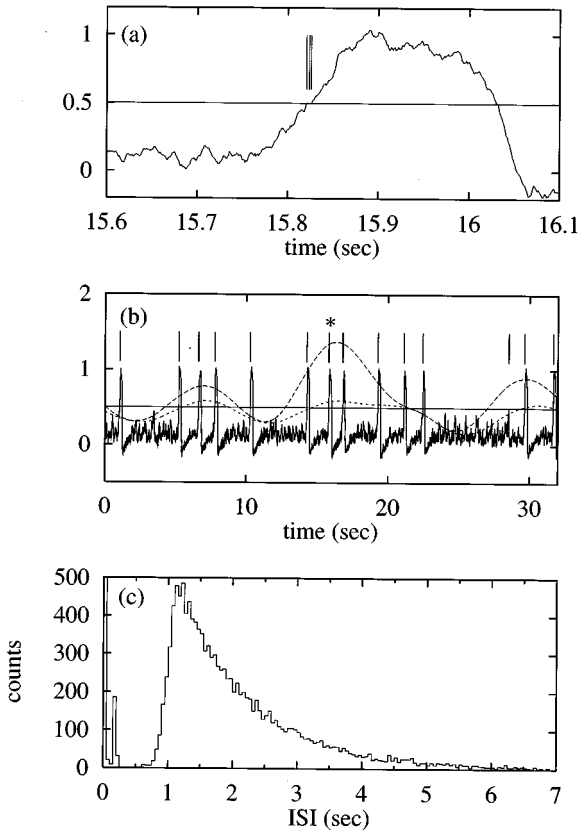

FIG. 1. (a) Detailed view of the action potential labeled by an asterisk in panel (b). The apparently single upward threshold crossing is in fact a close succession of three threshold crossings, each marked by a vertical bar. (b) Fast membrane potential $v(t)$ (continuous line), spikes times (marked by a vertical bar), and instantaneous firing rates (dashed lines) as defined in the text. The larger amplitude firing rate is obtained by counting all threshold crossings. (c) Interspike interval histogram. The intervals smaller than 0.5 sec are calculated from one or two false spikes. Time (here in sec) can be rescaled to match, e.g., action potential durations in an experimental setting.

a model of a nerve fiber of a certain length based on Eq. (2.1), the only threshold crossings that can be detected along the fiber are the ones corresponding to the action potential [11]. Therefore, an additional criterion is needed to detect only the biologically relevant spikes that propagate and transmit information about the input. Thus, we slightly modify the method in [8] by introducing, as in [12], an absolute refractory period (0.4 sec) wherein no positive-going threshold crossing is considered an action potential. In the context of Fig. 1(a) this criterion would assign the time of occurrence of the action potential to the first crossing rather than the third, with a negligible error of ≈ 5 msec. The more problematic false spikes are the ones that can occur during the action potential downstroke, and are eliminated using this criterion.

To illustrate the differences between the two spike-detection schemes, Fig. 1(b) shows 32 sec of a simulation of the FHN equations, Eq. (2.1). The noise intensity is $D=3\times10^{-6}$, and the signal was held constant at $S=0$. The upward crossings of the firing threshold (set to 0.5) are marked with vertical lines. The dashed lines draw the instantaneous firing rate; the upper one is calculated from the scheme without absolute refractory period, while the lower one disallows spikes closer in time than 400 msec. The difference in firing rates is striking; these differences increase with higher noise intensities (not shown).

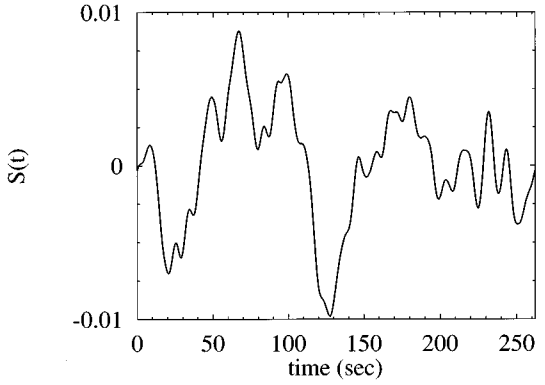

FIG. 2. Time series of the aperiodic signal used in our simulations.

Figure 1(c) shows the interspike interval histogram (bin width of 50 msec) constructed from a simulation of total time of 26 214.4 sec with the same parameters and constant input. There are 3157 intervals in the first bin (clipped in the plot). The intervals measured between acceptable action potentials follow a sharp γ-like distribution with a sharp rise at about 1 sec, and are clearly distinct from those (<0.5 sec) caused by small fluctuations around the threshold. Our choice of the absolute refractory period (0.4 sec) discards the ''false'' spikes without affecting the dynamically relevant events. In the following, we will compare results for simulations with and without an absolute refractory period in the spike-detection scheme. The proper consideration of these false spikes changes the conclusions of our paper quantitatively rather than qualitatively.

III. REPLICATING ASR AND SR WITHOUT TUNING

In this section, we reproduce the simulations as reported by Collins *et al.* [6,7,13]. The aperiodic signal $S(t)$ was constructed according to [6], that is, an OU process Eq. (2.2) with correlation time $\tau_c=20$ sec passed through a unit-area symmetric Hanning window filter of width 10 sec. Note that the Hanning window acts as an additional low-pass filter, resulting in a relatively smooth signal. It is important to realize that the correlation time of such a signal is much larger than any relevant time scale of the dynamical system Eq. (2.1). The one realization of the signal we use in all our simulations is shown in Fig. 2. The signal has zero mean, a variance of 1.5×10^{-5}, and a duration of 262.144 sec, a value that allows use of the fast Fourier transform (FFT) algorithm.

To compare our simulations with those in [6], we also use the ''power norm'' C_0 and the ''normalized power norm'' C_1 to measure the coherence between the signal $S(t)$ and the output $R(t)$. These quantities are defined as

$$C_0=\overline{S(t)[R(t)-\overline{R(t)}]} \tag{3.1}$$

and

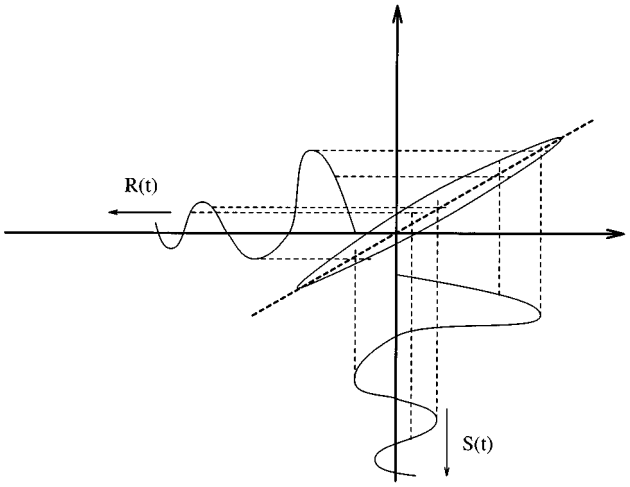

FIG. 3. Estimation of the covariance C_0 and correlation coefficient C_1 between $S(t)$ and $R(t)$. C_0 measures the mean slope, indicated by the slanted dashed line, of a hypothetical transfer function between the input $S(t)$ and the output instantaneous firing rate $R(t)$. C_1, a measure of the linearity of the transfer function, is sensitive to the slope variability around the slanted dashed line (see arcs below and above this line), and to the variance of $S(t)$ and $R(t)$.

$$C_1=\frac{C_0}{[\overline{S^2(t)}]^{1/2}\{\overline{[R(t)-\overline{R(t)}]^2}\}^{1/2}}. \tag{3.2}$$

The quantities in the denominator of Eq. (3.2) are the standard deviations of the signal and of the instantaneous firing rate. Note that, in fact, since $S(t)$ has zero mean, C_0 and C_1 are, respectively, the standard covariance and linear correlation coefficient [14]. In this sense, C_0 is proportional to the mean slope of a linear regression between S and R. C_1 measures the linearity of the input-output relationship of the neuron (see Fig. 3), and varies between -1 and 1, values for a perfect linear relationship with, respectively, negative or positive slope. C_1 is also proportional to C_0, and inversely proportional to the variances of S and R.

A. Replicating ASR

Figure 4 shows ensemble-averaged values and standard errors of C_0 and C_1 at different noise intensities D calculated using 300 realizations of the full dynamics Eq. (2.1), reproducing Fig. 1 in [6]. Circles with error bars label results obtained *without* an absolute refractory period in the spike-detection scheme, whereas squares are for results from the same realizations, but disallowing spikes closer in time than 400 msec. The best correspondence with the results in Fig. 1 of [6] is for the curves *without* an absolute refractory period. It is interesting that the rapid rise of C_0 to a clear peak with subsequent decay is less prominent when considering only physiologically relevant spikes. However, this also produces higher values of C_1.

To understand the full significance of these results, we have also plotted C_1 for all the individual runs (Fig. 5) used to calculate the mean and standard errors shown in Fig. 4. Only the values for simulations with absolute refractory period are shown. Even for the noise level at the ''resonant peak'' in Fig. 4, the distribution of C_1 values (and thus of C_0) is extremely broad, always encompassing realizations with negative correlation between output and input. Subtleties like spike-detection scheme do not substantially change this broad distribution (not shown). Hence, the standard error

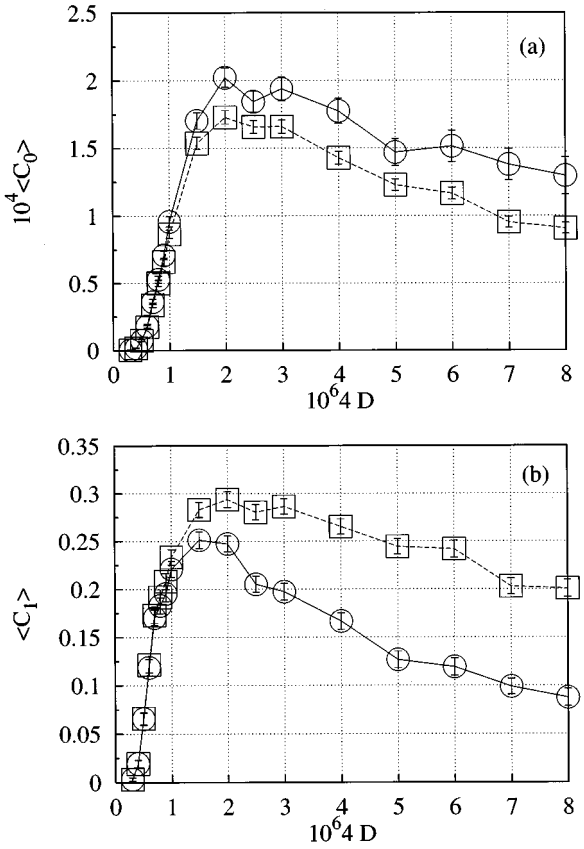

FIG. 4. Ensemble-averaged values and standard errors of the (a) covariance C_0 and (b) correlation coefficient C_1 versus noise intensity D for simulations of the full dynamics Eq. (2.1). Circles with error bars show C_0 and C_1 values for a spike-detection scheme without absolute refractory period. Squares denote values obtained by disallowing any spike that occurs within 400 msec of a previous spike.

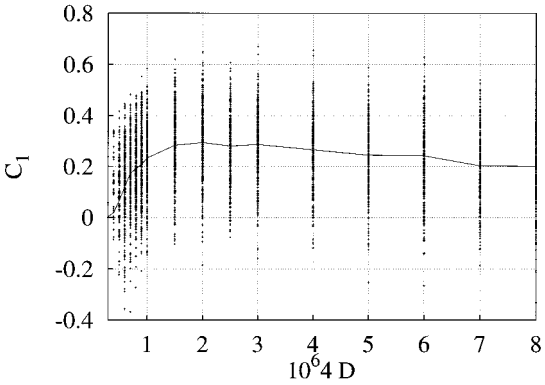

FIG. 5. Individual C_1 values from the 300 runs whose mean and standard error are shown in Fig. 4. Even in the best case ($D=1.5\times10^{-6}$; see Fig. 4) the spread is extremely large, with occasional realizations where input and output are anticorrelated.

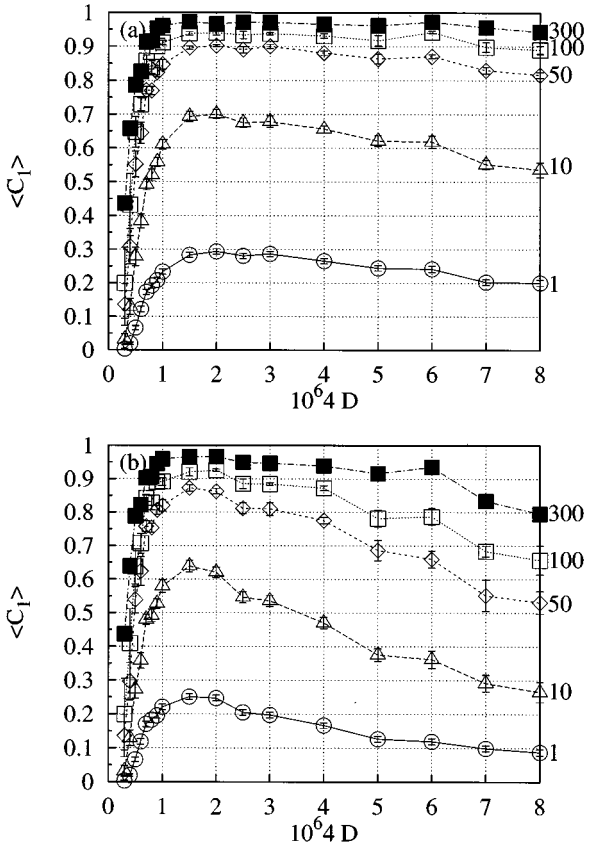

FIG. 6. ''SR without tuning.'' (a) C_1 versus D for different numbers of neurons acting in parallel, using the spike-detection scheme with absolute refractory period. Lines from bottom are for architectures with 1, 10, 50, 100, 300 neurons. Error bars denote the standard error on C_1 for, respectively, 300, 30, 6, 3, and 1 realizations. (b) Same as in (a), but *without* a refractory period in the spike-detection scheme.

(an error bar inversely proportional to the number of realizations) of C_0 and C_1 does not give as accurate a picture of the correlation as the standard deviation calculated across all realizations.

B. Replicating ''SR without tuning''

We now reproduce the results reported in [7] for neurons in parallel. As in [7], we consider an architecture where the output of individual neurons, each driven by the same input signal but a different noise source (the noise sources have zero cross correlation), is averaged before the correlation is measured. The averaged output $R_M(t)$ is

$$R_M(t)=\frac{1}{M}\sum_{i=1}^{M} R^i(t), \tag{3.3}$$

where $R^i(t)$ denotes the instantaneous firing rate of neuron i. Figure 6 shows results for $M=1$, 10, 50, 100, and 300 neurons in parallel and for both spike-detection schemes. While in both cases C_1 approaches 1 with increasing M, the case where only physiologically relevant spikes are counted is clearly superior in performance. The close similarity of Fig. 6 to [7], Fig. 2, again suggests that no refractory period was used in their reported simulations.

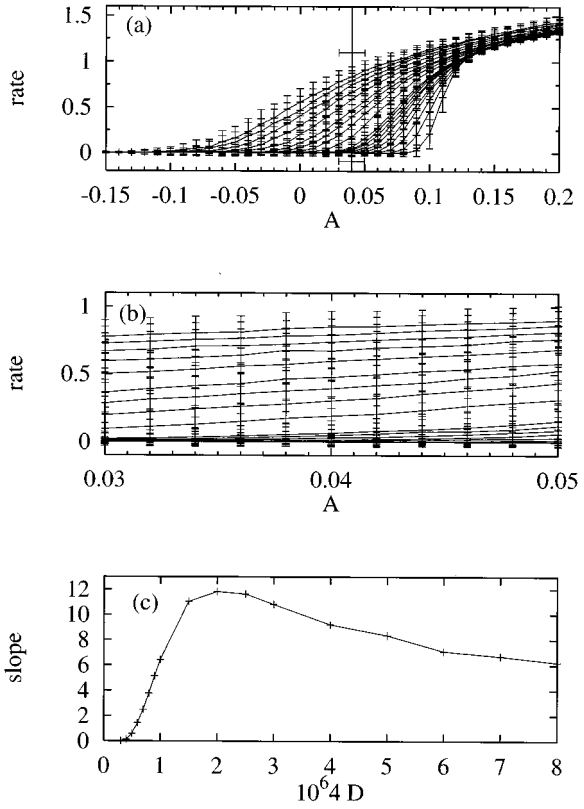

FIG. 7. Mean firing rate as a function of A determined by solving Eq. (2.1) numerically at different D values. The instantaneous firing rate $R(t)$ was computed at each integration time step from the resulting spike train, using a 10 sec Hanning window, taking a refractory period into account. The mean rate was then computed from the time average of $R(t)$. (a) Wide range of A. A Hopf bifurcation occurs for $0.113 \leqslant A_T \leqslant 0.114$. The signal range for the ASR simulations is indicated by the horizontal bars centered on $A=0.04$. (b) Same as in (a), but restricted to the range of A modulated by the signal. (c) Slope of the rate-versus-A curves in (b) as a function of D, determined by linear regression. Minimum noise intensities are $D=10^{-7}$ in (a) (rightmost curve) and $D=3\times10^{-7}$ in (b) (bottom curve), increasing by 10^{-7} up to 10^{-6}, then in steps of 5×10^{-7} up to 3×10^{-6}, and finally in steps of 10^{-6} up to 8×10^{6} (uppermost curves). Error bars in (a) and (b) denote the standard deviation (not the standard error). Ten sweeps of 157.3 sec were used for each parameter set in (a) [ten sweeps of 524.3 sec in (b)].

IV. NEURON TRANSFER FUNCTION

Our aim in this section is to explain ASR in terms of frequency modulation of the mean firing rate by the slowly varying input signal. We begin by computing the behavior of the firing rate as a function of tonic activation A and noise intensity D. This yields a basic transfer function for constant signals. The intuition behind our explanation of ASR is that the signal, varying on a time scale slower than all characteristic times of the stochastic neurons, produces quasistatic variations in the parameter A. Consequently, the firing rate observed near a given value of the input signal can be estimated from the transfer function at the corresponding (constant) value of A.

In Fig. 7(a), the mean firing rate for one neuron, governed by Eq. (2.1) with $S=0$, is plotted versus A for $D=10^{-7}$

(rightmost curve) to $D=8\times10^{-6}$ (leftmost curve). A supercritical Hopf bifurcation of the deterministic (i.e., noise-free) system from a fixed point to an oscillatory state occurs for $0.113\leqslant A\leqslant 0.114$ as in [6]. These rate curves were obtained by sampling the instantaneous firing rate from a total of 1573 sec of simulation for each combination of A and D. The mean firing rate is seen to always increase with increasing A and/or D. In the absence of noise, the rate is zero until $A\approx 0.113$, then jumps abruptly to a value near 1, and increases almost linearly thereafter. These results are compatible with work in the past decade aimed at characterizing analytically and numerically such rates of noise-induced firing for simple excitable systems [15,16].

In the ASR simulations, A is held constant at 0.04, and the signal varies by ± 0.01. This range of modulation of A induced by the signal [note that S and A are added together in Eq. (2.1)] is indicated in Fig. 7(a). For $A=0.04$, the autonomous deterministic dynamics correspond to fixed point behavior. As the dynamics are excitable, spikes can occur when the noise drives the state variables to the threshold for spiking. Our quasistatic description of ASR amounts to considering that the slow signal modulates the value of this globally stable fixed point.

Figure 7(b) gives an expanded view of the parameter range corresponding to the modulations produced by the signal. Conventions are the same as in Fig. 7(a), except that the total simulation time is now 5243 sec, and $3\times10^{-7}\leqslant D\leqslant 8\times10^{-6}$. From these data, the slope of the mean firing rate versus activation A for all D can be determined by linear regression. The relationship is almost linear for all curves (correlation coefficient >0.9 for $D\geqslant 5\times10^{-7}$ and >0.95 for $D\geqslant 8\times10^{-7}$).

These slopes are plotted as a function of D in Fig. 7(c). This is the basic transfer function of the neuron for constant and slowly varying signals, as they occur in ASR. The slope rapidly rises to a maximum at $D=2\times10^{-6}$, and decreases slowly thereafter. Within a constant scaling factor, this curve perfectly matches that of C_0 in Fig. 4(a). It is obvious from this curve that there is an optimal value of D for which the slope of the rate-vs-A relationship, or ''gain,'' is maximum. Together with the variance of the firing rate, this gain function allows us to predict the expected values of C_0 and C_1 for slow signals. The effect of noise here is to linearize the transfer function. Stochastic resonance, by contrast, is *not* a linearization [17] but a cooperative effect of signal and noise, when the time scale of the signal is commensurate with the noise-induced firing rate.

V. DERIVING C_0 AND C_1 FROM THE TRANSFER FUNCTION

A. Aperiodic stochastic resonance

We now derive the expected values of C_0 and C_1 for ASR from the characteristics of the rate-vs-A transfer function computed in Sec. IV. The shape of the transfer function in the activation range covered by the signal suggests, in the context of quasistatic signals, the following linear ansatz:

$$R(t)=\lambda_D S(t)+\eta_D(t), \tag{5.1}$$

where λ_D is the gain (slope) of the transfer function for noise intensity D, and η_D is a stochastic variable. This relation is similar to the one used in [6], with the substitution $\langle R(t)\rangle=\lambda_D S(t)$. With the ansatz Eq. (5.1), the expected value for C_0 is

$$\begin{aligned} E[C_0]&=\overline{S(t)[\lambda_D S(t)+\eta_D(t)]}\\ &=\lambda_D \mathrm{var}(S) \end{aligned} \tag{5.2}$$

under the assumption of vanishing correlation between the stochastic variation $\eta_D(t)$ and the signal. Here var(S) means ''variance of S.'' We plotted this relationship for both spike-detection schemes in Fig. 8(a). The match is excellent. The expected C_1 values can be derived by taking into account the variance of the stochastic variation of the linear transfer function. Starting again from the linear relationship, Eq. (5.1), and noting that

$$\mathrm{var}(R)=\lambda_D^2\mathrm{var}(S)+\mathrm{var}(\eta_D) \tag{5.3}$$

it follows that

$$\begin{aligned} E[C_1]&=\frac{E[C_0]}{\sqrt{\mathrm{var}(S)\mathrm{var}(R)}}\\ &=\frac{\lambda_D\mathrm{var}(S)}{\sqrt{\mathrm{var}(S)[\lambda_D^2\mathrm{var}(S)+\mathrm{var}(\eta_D)]}}\\ &=\frac{1}{\sqrt{\left(1+\dfrac{\mathrm{var}(\eta_D)}{\lambda_D^2\mathrm{var}(S)}\right)}}. \end{aligned} \tag{5.4}$$

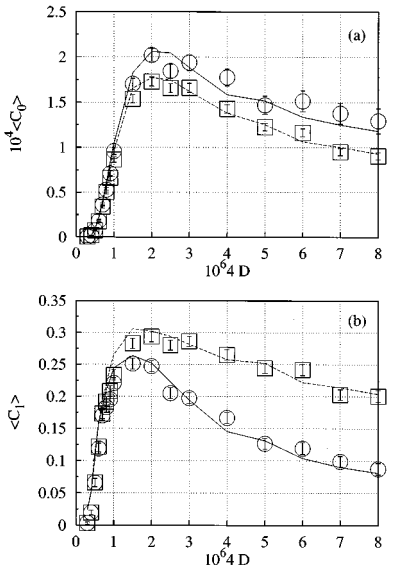

FIG. 8. Theory and simulation results of the (a) covariance C_0 and (b) correlation C_1 versus noise intensity D for simulations of the full dynamics Eq. (2.1). Circles with error bars show the results obtained without absolute refractory period, and squares are from simulations with a 400 msec refractory period (same data as in Fig. 4). The lines connect values of C_0 and C_1 computed using the transfer function and Eqs. (5.2) and (5.4) (see text).

In order to compare this expression for C_1 with the values derived from numerical simulations of the FHN equations with signal $S(t)$, it is necessary to estimate var(η_D). Noting that $S=$const in Eq. (5.3) yields var(R)=var(η_D), we can estimate var(η_D) from simulations with constant signal. Consequently, for a given value of D, var(η_D) is computed by averaging the sample variance of the instantaneous rate over $0.03<A<0.05$. For each value of A, the sample variance of the firing rate was taken from Fig. 7(b). Figure 8(b) shows the resulting values of C_1 for both spike-detection schemes. It is clear that the nonmonotonic character of C_1 vs D can be derived from the assumption of a noisy linear relationship between firing rate and tonic activation. This is the main result of our paper. For lower noise levels, the predicted values are slightly higher than the ones obtained from simulating the full dynamics. This is because, in this range of noise, the assumption of linearity is an approximation, as one can see from the slight curvature in the transfer function. Another contributing factor to the discrepancy is the fact that var(η_D) shows a systematic increase with A at low noise. However, the peak in our quasistatic estimate of C_1 as well as its decrease at higher noise levels are perfectly well explained by the linear ansatz.

It is interesting to note that the Kramer's-type analysis of the crossing rate of the FHN model presented in [6] supports our simple theory. This analysis, which approximates the escape-to-threshold problem in the two-dimensional FHN system by a one-dimensional one along the v axis, relies on the assumption of slow signals. While such adiabatic theories of stochastic resonance have been proposed [17], the fact that an adiabatic theory for the transition rates agrees with numerical results of course does not imply that the underlying phenomenon is stochastic resonance. We begin with Eq. (12) in [6] for the mean threshold-crossing rate in the presence of the slow aperiodic signal $S(t)$:

$$\langle R(t)\rangle \propto \exp\{-\sqrt{3}[B^3-3B^2S(t)]\epsilon/D\}, \tag{5.5}$$

where $B\equiv A_T-A$ measures the distance between the signal mean and the threshold (in [6], A_T is a constant equal to ≈ 0.11, i.e., the bifurcation value found numerically above). Plots of $\langle R\rangle$ as a function of the tonic activation A for constant signal and constant D are similar to those in Fig. 7(b), and also behave similarly as D is changed (not shown). The partial derivative of this rate with respect to A then yields the slope, similar to λ_D:

$$\frac{\partial\langle R\rangle}{\partial A} \propto \frac{3\sqrt{3}\epsilon}{D}(A_T-A)^2 \exp\left[-\frac{\sqrt{3}\epsilon}{D}(A_T-A)^3\right]. \tag{5.6}$$

Plots of $\partial\langle R\rangle/\partial A$ as a function of D for constant A exhibit the familiar unimodal shape seen in Fig. 7(c), since this quantity has an $\exp(-1/D)/D$ dependence. Further, we see that this slope or ''gain'' goes to zero at very high noise, as expected from an extrapolation of the results of Fig. 7(b). This expression for the slope can then be substituted into Eq. (5.4) which, together with a numerical determination of var(η_D) vs D (e.g., a quadratic function in D as in [6,7]), can be used to determine C_1 as different D values.

The nonlinearity that underlies ASR can also be intuitively understood using a simple analogy with the transfer functions (so-called ''squashing'' functions) used in neural networks (see, e.g., [18]). Such functions represent the instantaneous firing rate f of a neuron as a function of its activation or input level x, a quantity similar to the activation level A above. This function goes to zero as $x\to-\infty$, and to the maximal firing rate (usually chosen to be one) as $x\to\infty$. A frequently used analytical form is $f=[1+\exp(-\beta x)]^{-1}$, a sigmoid whose slope at the origin is $f'(0)=\beta$. This sigmoid turns into a Heaviside step function as $\beta\to\infty$. This occurs when the noise level $D\equiv\beta^{-1}$, proportional to temperature in the neural network context, goes to zero. For any x, the slope is

$$\frac{df}{dx}=\exp(-x/D)D^{-1}[1+\exp(-x/D)]^{-2}. \tag{5.7}$$

For a given level of activation, this slope, which is similar to that of the curves in Figs. 7(a) and 7(b), starts at zero for $D=0$, goes through a maximum, and decays to zero as $D\to\infty$. This reproduces the basic behavior seen in Fig. 7(c).

B. Neurons in parallel

The linear ansatz also allows the prediction of C_0 and C_1 for multiple neurons in parallel. Taking Eq. (5.1) together with Eq. (3.3), we obtain for M neurons

$$R_M(t)=\frac{1}{M}\sum_{i=1}^{M} R^i(t)=\lambda_D S(t)+\frac{1}{M}\sum_{i=1}^{M}\eta_D^i(t), \tag{5.8}$$

where the $\eta_D^i(t)$ are different stochastic variables for each neuron and have zero cross correlation. We first remark that the expected value of C_0 is the same for a single neuron as for M neurons in parallel. Assuming then that the $\eta_D^i(t)$ have the same variance var(η_D), it follows that

$$\mathrm{var}(R_M)=\lambda_D^2\mathrm{var}(S)+\frac{1}{M}\mathrm{var}(\eta_D), \tag{5.9}$$

and thus, as for Eq. (5.4),

$$E[C_1^M]=\frac{1}{\sqrt{1+\dfrac{1}{M}\dfrac{\mathrm{var}(\eta_D)}{\lambda_D^2\mathrm{var}(S)}}}. \tag{5.10}$$

We tested the accuracy of this relation for $M=1$, 10, 50, 100, and 300 for both spike-detection schemes. The results are plotted in Fig. 9 together with results from simulations of the full dynamics. For the same reasons as in the single neuron case, the predicted values are slightly higher than those from the full simulations for $D<10^{-6}$, but match them very closely for higher D. Also, C_1 is again higher when a refractory period is taken into account.

This estimate of C_1 in Eq. (5.10) in terms of the single neuron parameters var(η_D) and λ_D goes to one with increasing M for $\mathrm{var}(\eta_D)/\lambda_D^2>0$, i.e., for nonvanishing noise intensity. As the value of C_1 for a signal of a given variance fed to M neurons in parallel is determined by the factor $\mathrm{var}(\eta_D)/(M\lambda_D^2)$, it follows that C_1 can be improved by increasing λ_D. Another way to increase C_1 is to increase the

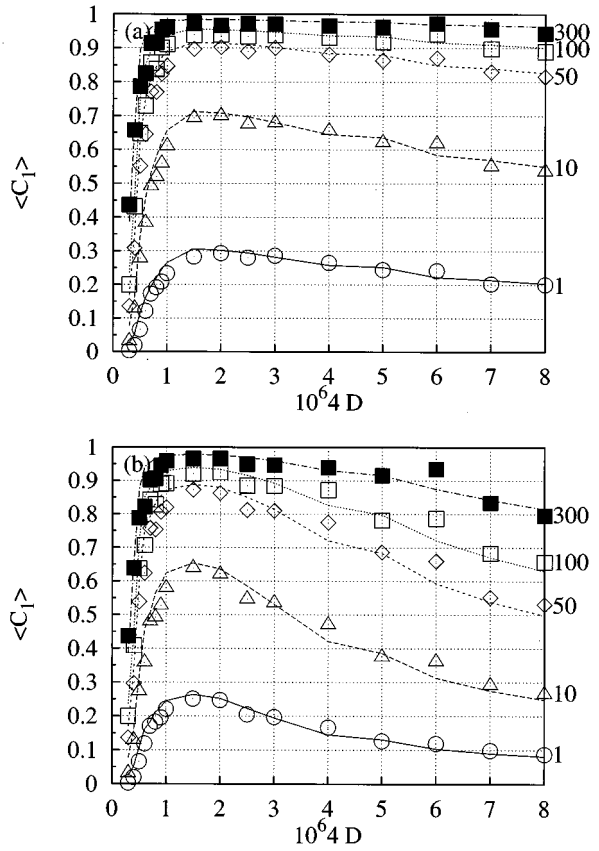

FIG. 9. ''SR without tuning'' explained using the transfer function in Fig. 7, with (a) and without (b) refractory period. Symbols are mean values obtained from simulating the full dynamics (see Fig. 6) (from bottom, for systems with 1, 10, 50, 100, and 300 neurons). Lines are theoretical values, calculated from Eq. (5.10). var(η_D) was estimated as in Fig. 8, i.e., by averaging across A values using the data in Fig. 7(b).

linearity of the transfer function over the relevant range of A values. It is tempting then to compare simulations of M neurons in parallel to one with a single neuron operating in a parameter range where the transfer function deviates very little from linearity. Such a parameter range occurs for $D=0$ and A close to but above the threshold value ≈ 0.114. In other words, a single neuron could also optimize its response to a slow aperiodic input by adapting its dynamics to a higher resting potential, or (from another point of view) by lowering its threshold.

To illustrate the notion that a single neuron can do as well as a summing network of neurons operating at a higher threshold, we compare the performance of 300 neurons, each with the same dynamical parameters and $A=0.04$, to a single neuron with all the same dynamical parameters, except $A=0.125$ and $D=0$. The single neuron now fires periodically in the absence of input signal and noise, since $A>0.114$. The value of $A=0.125$ is chosen such that the C_1 value for the single deterministic neuron equals the maximum value obtainable in the noisy summing network, namely, that for $D=1.5\times 10^{-6}$. A comparison of $S(t)$ with $R(t)$ for the single deterministic neuron in its suprathreshold regime and $R_M(t)$ for the 300 noisy neurons is shown in Fig. 10. Thus, a shift in membrane potential to a region of linearity also optimally transduces a slow aperiodic signal. This is

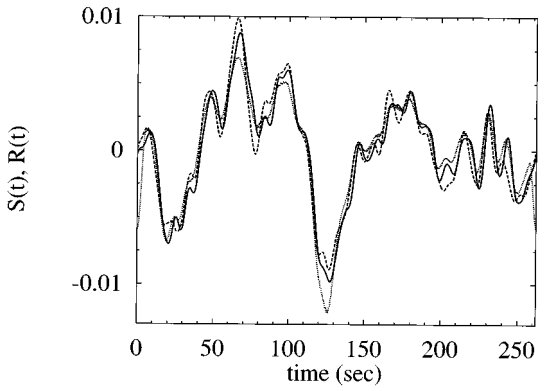

FIG. 10. Comparison of rate coding of a slowly varying signal (solid line) by a single noiseless suprathreshold neuron and a summing network of subthreshold noisy neurons. The dashed line represents $R_M(t)$ from the average activity of 300 neurons ($A=0.04$, $D=1.5\times 10^{-6}$, for a total of 14 803 spikes), as in the *stochastic resonance without tuning* scenario. The dotted line is $R(t)$ from a single neuron in the suprathreshold regime ($A=0.125$, $D=0$, 272 spikes). The correlation coefficients are $C_1=0.96$ for the 300 stochastic neurons, and $C_1=0.957$ for the single deterministic neuron, respectively.

true here even though the mean slope of the transfer function with noise is actually higher than without noise. The reason why C_1 is not exactly one for the single neuron is that there is a slight curvature in the noiseless rate-versus-A function.

The analysis in [6] relies on the assumption $[\overline{S^2(t)}]^{1/2} \ll B$, i.e., signal variance is much smaller than signal-to-threshold distance. For large B, i.e., for signals near or above threshold, it may adequately approximate values of C_1. On the other hand, our transfer function analysis allows us in principle to predict, for any value of A (and thus, of B), the value of C_1 for one or many neurons driven by a slowly varying aperiodic input. The accuracy of our prediction will be higher if the slope of the transfer function is almost constant across the relevant range of A values. This linearity will depend on the minimum and maximum bounds of the signal amplitude, as well as on the particular combination of A and D values used.

It is clear that the reduction of the noise variance achieved using the summing network broadens the range of noise intensities for which C_1^M is high. This flattening of the C_1^M versus D curve will however be much more difficult to maintain as D increases. The theory presented in [6] yields an analytical approximation to C_1. This result has been extended to M neurons by recalculating the normalization factor N^2 in the denominator of C_1 [N^2 is the variance of $R(t)$]. The result is

$$N_M^2 \equiv \mathrm{var}(R_M) = \overline{\langle R\rangle^2} - \overline{\langle R\rangle}^2 + \sigma^2(D)/M, \qquad (5.11)$$

where brackets denote ensemble averages, overbars denote time averages, and $\sigma^2(D)$ is simply var(η_D) used throughout our study. This factor is then used to obtain C_1^M [see Eq. (3) in [7]]. For large D, and assuming that the Kramers rate approximation is still valid, this expression goes as $\sqrt{M}/D\sigma(D)$. Assuming that σ^2 maintains its quadratic dependence on D, and that the noise sources on the neurons

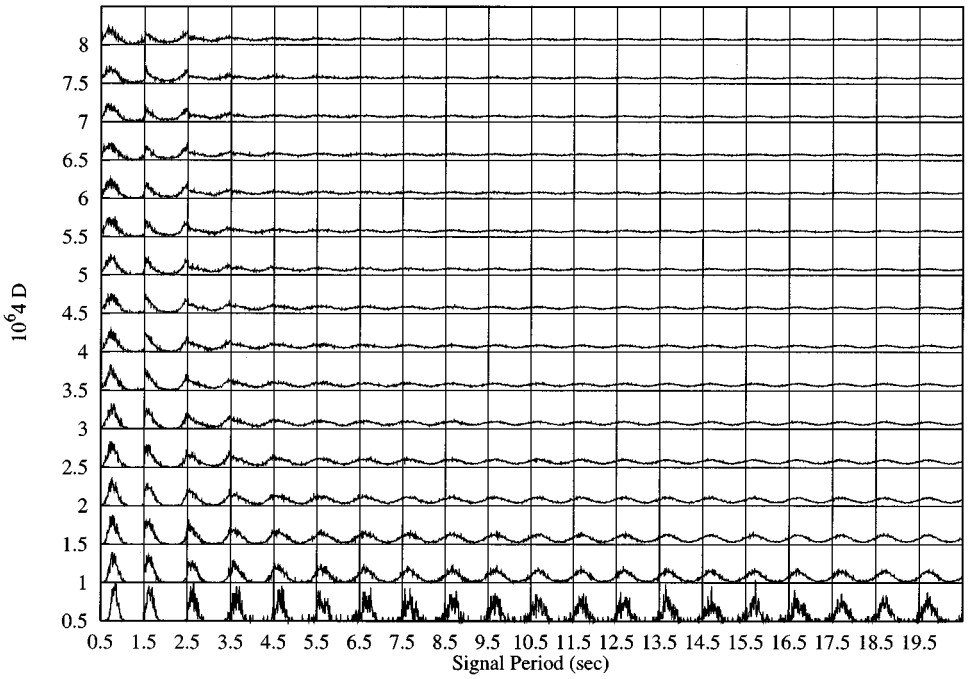

FIG. 11. ''Cycle histograms'' for different noise intensities and signal periods. Each box represents a histogram computed for values of noise intensity and signal period indicated on the axes. In each box the firing probability (full scale corresponds to P between 0 and 0.15) is plotted versus the phase (full scale corresponds to phases from 0 to 2π) of the periodic signal. Histograms depicted here were used to compute the correlation coefficients plotted in Fig. 12.

indeed remain uncorrelated, we find that $C_1^M \approx \sqrt{M}/D^3$. This implies that, e.g., for a twofold increase in the noise level, a high value of correlation obtained with M neurons can be maintained by using instead $64M$ neurons. We note that the same scaling is obtained using our Eq. (5.10), in combination with Eq. (5.6), since this latter equation yields a $1/D$ dependence of λ_D at large D. Thus, broadening of C_1 versus D will occur, but can be quickly overcome by increased noise.

VI. LOOKING AT THE FREQUENCY-NOISE INTENSITY PARAMETER SPACE

In this section we investigate the correlation of the firing rate with subthreshold periodic signals of varying frequency for different noise intensities. Our aim is to illustrate that there are regions in parameter space where linearization by noise governs the behavior of C_1, and others regions where stochastic resonance plays a role.

The correlation C_1 was computed between a sinusoid and a histogram representation of $R(t)$ over one stimulus cycle. This is known in the neurophysiology jargon as a ''cycle histogram,'' and represents (after proper normalization) the probability of occurrence of a spike as a function of the phase of the periodic signal. These histograms were computed from numerical simulations of Eq. (2.1) as before, except that here $S(t)$ is a sinusoid of amplitude 0.01 (comparable with that of the aperiodic signal used in previous sections) and period T ranging from 20 sec to 0.5 sec. The noise intensity ranges from 0.5×10^{-6} to 8×10^{-6}.

For each noise intensity-signal period combination, the firing phases of the spikes were computed from 3200 realizations of each period, i.e., from 3200 cycles of the signal. The refractory period was taken into account in the detection scheme, as explained in Sec. II. The histograms were computed by dividing one cycle of the signal into 100 bins. Note that this criterion of choosing a constant number of bins should be taken into consideration for the interpretation of the results in this section. For comparison with the treatment of $R(t)$ used in previous sections, phase histograms here can be considered equivalent estimates of rate functions over one cycle, obtained by convolving the spike trains with nonoverlapping rectangular windows of length $T/100$, with results over all cycles folded modulo 2π into one cycle. The resulting number of counts in each bin of the cycle histogram is further divided by the total number of spikes encountered during the 3200 cycles, producing a normalized cycle histogram. Under these conditions, results in this section can also be seen as analogous to the ensemble-averaged rate of 3200 neurons in parallel over one stimulus cycle. We note that the value of C_1 is not affected by the normalization.

Figures 11 and 12 show the result of our simulations of Eq. (2.1) with subthreshold periodic forcing. It is clear that high values of correlation can be seen over the whole range of stimulus periods studied. Let us focus first on the parameter values of Fig. 11 which yield ''half-wave rectified'' histograms. These cases occur for the lowest noise intensities and all periods, and for the shortest periods and all noise intensities (in other words, for the cases along the x or y axes). For these parameter combinations, there is a higher probability of firing near a given phase of the sinusoidal input, and very little firing over a range of phases of $\approx\pi$ rad. As noise or period increases, i.e., as one moves away from the x or y axes, the histogram resembles more and more the sinus input. This qualitative observation can be confirmed by looking at the respective values of C_1. These values of C_1, shown in Fig. 12, represent the highest value of correlation between the cycle histogram and a sinusoid of period T, the phase of which can be varied across $(0,2\pi)$. As is already apparent from visual inspection, the amount of phase shift leading to this maximal correlation depends on the noise intensity and the signal period.

We have observed that, for all the parameter values resulting in ''rectification'' in the cycle histogram, the individual spike trains exhibit the typical ''skipping'' behavior

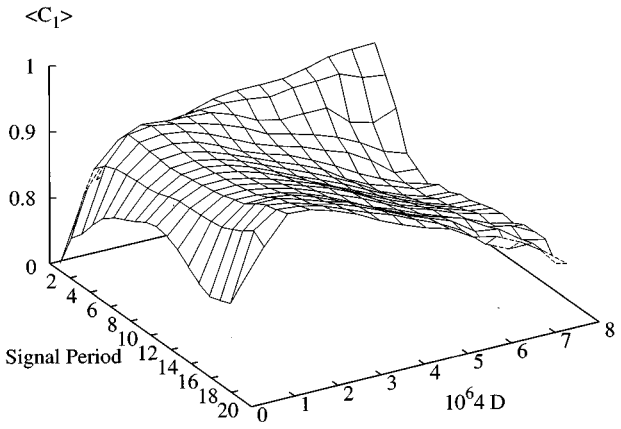

FIG. 12. Correlation coefficient as a function of the period T of the sinusoidal signal (sec) and the noise intensity. The correlation C_1 for given values of D and T is measured by first constructing a cycle histogram (i.e., a histogram of firing probability over one period of the stimulus; see Fig. 11). C_1 is then computed between this cycle histogram and a sinusoid for different phase shifts in $(0,2\pi)$. C_1 values plotted here correspond to the maximum correlation across all phase shifts.

[3], and consequently, multimodal interspike interval histograms (not shown). It is important to remark that this is the hallmark of ''a nonlinear cooperative effect whereby the small signal entrains the noise-induced hopping, so the transitions are surprisingly regular'' [17] (see also [2,19]). This extreme regularity associated with rectification, i.e., firings occurring only near a given phase of a periodic input, would prevent a neural ensemble from encoding the full excursions of the signal, resulting here in relatively low C_1 coefficients. This result implies that proper encoding, where the rate follows every modulation of an aperiodic input signal, requires a relatively larger noise intensity (for a given fixed period) than those producing the ''surprisingly regular'' noise-induced hopping, i.e., than those associated with skipping.

For relatively long signal periods, the behavior of C_1 as a function of D (see Fig. 12) is, not surprisingly, similar to what was shown in previous sections for aperiodic signals. Note also, in Fig. 11, the decrease in the amplitude of the sinusoidal modulation of the cycle histogram with increase D. This is due to the nonlinear decrease of the gain with increasing noise discussed in Sec. IV and V.

It is thus clear that, for any frequency, the correlation exhibits a clear maximum as D is increased. It is further observed that for periods corresponding to the slow inputs used in ASR, the maximum always occurs near the same value of $D \equiv D_{max}$. However, for $T<2$ sec, the maximum moves to higher values of D. This increase in D_{max} is a clear signature of stochastic resonance, and can be understood from the time-scale matching notion of SR [17,2,8]: a higher noise level produces a higher mean crossing rate, which will optimally transduce a subthreshold deterministic signal of higher frequency. We note that this dependence of D_{max} on frequency in the FHN system is more pronounced than for the maximum in SNR in the dynamically simpler two-state double-well system studied, e.g., in [19]. This is probably due to the (slower) time scale associated with the recovery variable in Eq. (2.1).

VII. CONCLUSION

In summary, our analysis shows that the *aperiodic stochastic resonance* and *stochastic resonance without tuning* scenarios do not rely on the nonlinear cooperative effect of stochastic resonance, but rather on the noise dependence of a linearization-by-noise effect. The role of noise in ASR is simply to linearize the transfer function of the neuron, i.e., the fundamental relationship between the input to the neuron, $S(t)$, and the instantaneous output firing rate of the neuron, $R(t)$ (Fig. 7). A slowly varying signal increases the neuron firing rate in proportion to its amplitude, i.e., the neuron encodes the signal through rate coding. This fact, along with the transfer function, enabled us to derive expressions for the expected covariance C_0 and correlation coefficient C_1 between S and R. C_0 is simply the gain of the encoding. C_1 measures the quality of a straight line fit to the transfer function of the neuron, and hence will be higher the more linear the transfer function is. It is important to stress that the optimal noise level is not exactly the one for which the input-ouput transfer function has the largest gain λ_D. Rather, λ_D enters into Eq. (5.4), and it is this expression which determines the maximal value of C_1 as a function of D. This determination requires, in our study as in [6,7], a numerical determination of var(η_D).

We have taken special care to reproduce the numerical results of previous studies [6,7] in order to carry out our study of the nonlinearity underlying ASR in single neurons and in summing networks. In particular, we have found that disallowing false spikes produces more coherence between output firing rate and input signal. Thus, there is some benefit to introducing a refractory period in the simulations, and perhaps for the existence of a refractory period in real neurons. Also, we have found that using the standard deviation rather than the standard error for the estimates of correlation gives a better assessment of the degree of correlation. In fact, while the mean value of C_1 may be positive, typical realizations may show negative correlation between output firing rate and input signal.

Although the high C_1^M values for the summing networks do not rely on stochastic resonance, it is still true that their averaging property reduces the variability of the instantaneous firing rate. Consequently, the C_1-versus-D curve does have a broader maximum, as Eq. (5.10) and the analysis in [6,7] predicts. As a wider range of noises then allows encodings of similar quality, the noise does not have to be tuned as critically as for optimal ASR in one neuron [6]. It is important to realize, however, that an optimal C_1 for ASR does not imply a tuning of time scales between system and signal, since the signal evolves on the slowest time scales. We anticipate that it will be possible to obtain ''true ASR'' for aperiodic signals evolving on time scales where SR occurs, i.e., for signals with a higher frequency content (the left of Fig. 12).

A recent study [20] of ''SR'' in threshold systems without dynamics concluded that the effect is more correctly interpreted as a special case of dithering, i.e., threshold crossing aided by noise. This result holds for forcing frequencies much lower than the noise bandwidth, and is said to apply to nonperiodic signals as well. For periodic forcing, such systems have only one time scale (i.e., the forcing), and thus no

time-scale matching is possible. That work also showed that a quantity measuring the deviation from linearity of the function relating averaged output and input goes through a minimum as a function of noise, i.e., an optimal noise level best linearizes the input-output ''transfer'' function. These behaviors are similar to those seen in the present study of ASR in the neuron model with slow inputs, even though matching of deterministic and stochastic time scales is possible in such a two-dimensional dynamical system [8].

We note that there are also two very recent studies of ASR. The first is a numerical and theoretical demonstration of the effect in a bistable system, as well as in an integrate-and-fire and the Hodgkin-Huxley neuron models [21]. The second is an experimental demonstration of the effect in a mechanoreceptor [22]. As the conditions on the relative time scales of signal and system used in these studies are described to be the same as in [6,7], we anticipate that the results of our study are equally relevant to those findings.

Linearization by noise in neurons is a well-known effect that has been studied both theoretically and experimentally (see, e.g., the superb review [23], as well as those contained in [24]). The results presented here and in [6,7] provide a theoretical and numerical framework with which to understand the basis for achieving optimal transduction of slow inputs through variations in noise intensity. Future work will take a closer look at the tuning properties of noisy neurons in light of the conclusions of the present study.

ACKNOWLEDGMENTS

This work was supported by NIMH through Grant No. MH 50064 and by NSERC (Canada). The Santa Fe Institute receives funding from the John D. and Catherine T. MacArthur Foundation, the NSF (PHY9021437), and the U.S. Department of Energy (DE-FG03-94ER61951).

[1] F. Moss, A. Bulsara, and M. F. Shlesinger, J. Stat. Phys. **70**, 4 (1993).
[2] L. Gammaitoni, F. Marchesoni, and S. Santucci, Phys. Rev. Lett. **74**, 1052 (1995).
[3] A. Longtin, A. Bulsara, and F. Moss, Phys. Rev. Lett. **67**, 656 (1991).
[4] J. K. Douglass, L. Wilkens, E. Pantazelou, and F. Moss, Nature **365**, 337 (1993); A. Bulsara, S. Lowen, and C. Reese, Phys. Rev. E **49**, 4989 (1994); K. Wiesenfeld, D. Pierson, E. Pantazelou, C. Dames, and F. Moss, Phys. Rev. Lett. **72**, 2125 (1994); J. F. Lindner, B. K. Meadows, W. L. Ditto, M. E. Inchiosa, and A. Bulsara, *ibid.* **75**, 3 (1995); C. Kurrer and K. Schulten, Phys. Rev. E **51**, 6213 (1995); P. Jung and G. Mayer-Kress, Phys. Rev. Lett. **74**, 2130 (1995); J. Levin and J. P. Miller, Nature **380**, 165 (1996).
[5] Possibilities are that modifications of the threshold and/or the ''intrinsic'' noise can occur in the sensory neuron.
[6] J. J. Collins, Carson C. Chow, and Thomas T. Imhoff, Phys. Rev. E **52**, R3321 (1995).
[7] J. J. Collins, Carson C. Chow, and Thomas T. Imhoff, Nature **376**, 236 (1995).
[8] A. Longtin, J. Stat. Phys. **70**, 309 (1993).
[9] R. Manella and V. Palleschi, Phys. Rev. A **40**, 3381 (1989).
[10] R. F. Fox, Phys. Rev. A **43**, 2649 (1991).
[11] J. J. B. Jack, D. Noble, and R. W. Tsien, *Electric Current Flow in Excitable Cells* (Oxford University Press, Oxford, 1985).
[12] A. Longtin, Nuovo Cimento D **17**, 835 (1995).
[13] J. J. Collins (private communication).
[14] J. S. Bendat and A. G. Piersol, *Random Data* (Wiley, New York, 1986).
[15] C. Kurrer, Ph.D. thesis, University of Illinois at Urbana (unpublished).
[16] H. Treutlein and K. Schulten, Ber. Bunsenges. Phys. Chem. **89**, 710 (1985).
[17] K. Wiesenfeld and F. Moss, Nature **373**, 33 (1995).
[18] J. Hertz, A. Krogh, and R. G. Palmer, *Introduction to the Theory of Neural Computation*, Santa Fe Institute Studies in the Sciences of Complexity Vol. 1 (Addison-Wesley, Redwood City, CA, 1991).
[19] B. McNamara and K. Wiesenfeld, Phys. Rev. A **39**, 4854 (1989).
[20] L. Gammaitoni, Phys. Rev. E **52**, 4691 (1995).
[21] J. J. Collins, C. C. Chow, A. C. Capella, and T. T. Imhoff, Phys. Rev. E **54**, 5575 (1996).
[22] J. J. Collins, T. T. Imhoff, and P. Grigg, J. Neurophysiol. **76**, 642 (1996).
[23] J. P. Segundo, J.-F. Vibert, K. Pakdaman, M. Stiber, and O. Diez Martinez, in *Origins: Brain and Self Organization*, edited by K. Pribram (Lawrence Erlbaum Associates, Hillsdale, NJ, 1994).
[24] M. M. Millonas, *Fluctuations and Order. The New Synthesis* (Springer, New York, 1996).